Reprinted from JOURNAL OF ATMOSPHERIC AND OCEANIC TECHNOLOGY, Vol. 3, No. 3, SEPTEMBER 1986
American Meteorological Society

Multiwavelength Scanning Radiometer for Airborne Measurements of Scattered Radiation within Clouds

MICHAEL D. KING

Laboratory for Atmospheres, NASA Goddard Space Flight Center, Greenbelt, MD 20771

MAXWELL G. STRANGE, PETER LEONE AND LAMDIN R. BLAINE

Laboratory for Oceans, NASA Goddard Space Flight Center, Greenbelt, MD 20771

(Manuscript received 12 November 1985, in final form 17 March 1986)

ABSTRACT

A multi-wavelength scanning radiometer has been developed for measuring the angular distribution of scattered radiation deep within a cloud layer. The purpose of the instrument is to provide measurements from which the single scattering albedo of clouds can be derived as a function of wavelength. The radiometer has a 1° field of view and scans in the vertical plane from 5° before zenith to 5° past nadir (190° aperture). The thirteen channels of the cloud absorption radiometer are located between 0.5 and 2.3 μm and were selected to avoid the molecular absorption bands in the near-infrared. The first seven channels of the radiometer are simultaneously and continuously sampled, while the eighth registered channel is selected from among the six channels on a filter wheel. This paper describes the optical, mechanical and electrical design of the instrument and presents some early results obtained from measurements taken aboard the University of Washington's B-23 aircraft to illustrate the performance of the instrument.

1. Introduction

Theoretical calculations suggest that cloud absorption can approach 15%–20% of the incident solar radiation for the more absorbing and thicker clouds (Twomey, 1976; Stephens, 1978a,b; Slingo and Schrecker, 1982; Davies et al., 1984). Aside from the obvious climatic significance of such a major heat source in the troposphere, Twomey (1983) has suggested that the strong diurnal variation in both the magnitude and depth of penetration of this solar heating might be a major contributor to the sudden "burning off" of California stratus layers as the solar zenith angle decreases toward noon.

The principal observations that have contributed to our knowledge of the absorption of solar radiation by clouds have been obtained from broadband pyranometers flown above and below clouds. These observations are subject to large errors, since the derivation of fractional cloud absorption requires taking the residual of four large flux measurements. Furthermore, these observations are often hindered by the very practical restrictions on aircraft ceilings and air traffic corridors, making it difficult to obtain meaningful flux observations both above and below the same cloud layer. In spite of these limitations, aircraft observations by Reynolds et al. (1975), Herman (1977), Stephens et al. (1978) and Herman and Curry (1984) suggest significant absorption of solar radiation by cloud layers, often exceeding theoretical predictions for clouds composed solely of liquid water and water vapor. Anomalously large cloud absorption has also been reported by Rozenberg et al. (1974) and Twomey and Cocks (1982) using spectral remote sensing methods applied to radiation reflected by clouds.

This discrepancy between observations and theory led Twomey (1972, 1977) to suggest that absorbing aerosol particles may be partly responsible for the high absorption. Recent calculations by Newiger and Bähnke (1981) have shown that absorbing aerosol particles interstitial to the cloud droplets can enhance cloud absorption to values as large as 30% of the incident solar radiation. The possibility also exists that leakage of radiation through the sides of some clouds might account for some of the large values of absorption implied by the measurements. This explanation, however, seems unable to account for the anomalous absorption observations of Herman (1977), Stephens et al. (1978), Twomey and Cocks (1982) and Herman and Curry (1984), all of whom took care to collect data in stratiform cloud regimes far from the influence of cloud boundaries. Finally, Wiscombe et al. (1984) have suggested the possibility that very large drops in some clouds could contribute to larger absorption values than typically obtained from calculations.

As a consequence of the rather large discrepancies between observations and theory, we were prompted to develop an aircraft radiometer for measuring the

spectral single scattering albedo of clouds using a technique that avoids the difficulties of traditional radiometric observations. This radiometer measures the angular distribution of scattered radiation deep within a cloud layer at selected wavelengths in the visible and near-infrared. In this paper we briefly review the diffusion domain method for determining the spectral single scattering albedo of clouds (King, 1981), describe the optical, mechanical and electrical design of a new cloud absorption radiometer, and present initial results obtained from radiometric observations taken aboard the University of Washington's B-23 research aircraft.

2. Theoretical basis of experiment

For optically thick and horizontally extensive cloud layers it is possible to derive quantitative information about cloud absorption properties from the angular distribution of scattered radiation deep within a cloud layer. In this region, known as the diffusion domain, the diffuse radiation field assumes an asymptotic form characterized by rather simple properties. Mel'nikova (1978) was the first to suggest that the ratio of the upward to downward flux densities in the diffusion domain be used to determine the single scattering albedo of clouds. King (1981) demonstrated that the ratio of the zenith to nadir propagating intensities within a cloud layer is more sensitive than the ratio of flux density measurements for determining the spectral absorption properties of clouds. Furthermore, King showed that the ratio of the zenith to nadir propagating intensities is reduced solely to a function of surface albedo (A_g), cloud similarity parameter (s) and scaled optical thickness between the aircraft flight level and the base of the cloud [$(1 - g)(\tau_c - \tau)$]. The similarity parameter is, in turn, related to the cloud asymmetry factor (g) and the single scattering albedo (ω_0) through the relationship

$$s = \left(\frac{1 - \omega_0}{1 - \omega_0 g}\right)^{1/2},$$

where s reduces to $(1 - \omega_0)^{1/2}$ for isotropic scattering ($g = 0$) and spans the range 0 ($\omega_0 = 1$) to 1 ($\omega_0 = 0$).

Figure 1 illustrates the relative intensity $I(\tau, \cos\theta)/I(\tau, 1)$ as a function of zenith angle θ for various values of the similarity parameter s. The zenith angle is here defined with respect to the downward directed normal, such that $\theta = 0°$ corresponds to nadir propagating radiation and $\theta = 180°$ to zenith propagating radiation. This figure applies when observations are made at an optical depth $\tau = 32$ in a cloud of total optical depth $\tau_c = 64$ and when the ground albedo $A_g = 0.07$. These results were obtained using the phase function first introduced by Henyey and Greenstein (1941), where we have assumed a value of the asymmetry factor ($g = 0.84$) typical of clouds at midvisible wavelengths. Provided $\tau \geq 12$ and A_g and g remain unchanged, the results presented in Fig. 1 apply for all values of τ_c when $\tau_c - \tau = 32$.

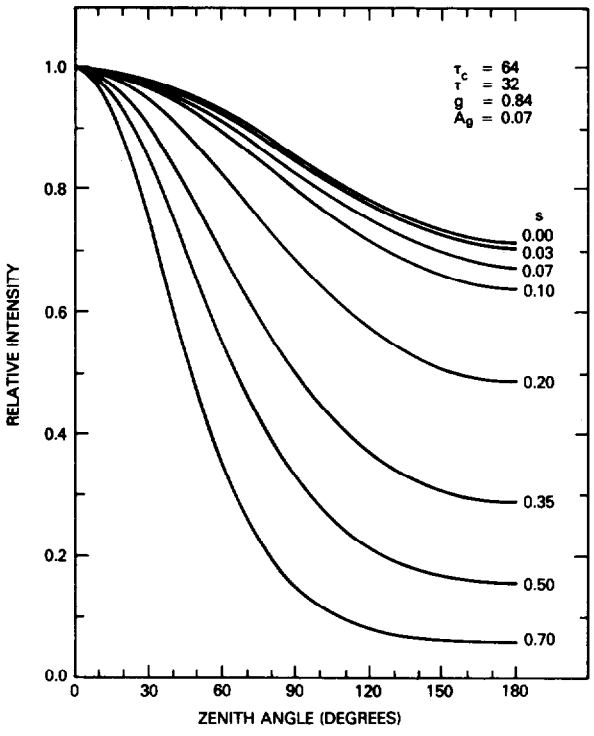

FIG. 1. Relative intensity as a function of zenith angle and similarity parameter at the midlevel of a cloud of optical depth $\tau_c = 64$. These curves apply for a Henyey–Greenstein phase function with $g = 0.84$ and when the surface albedo $A_g = 0.07$.

From the results presented in Fig. 1 we see that the relative intensity becomes more anisotropic as the similarity parameter increases, differing increasingly from the functional dependence $I(\tau, \cos\theta) = a + b\cos\theta$ required for conservative scattering ($\omega_0 = 1$, $s = 0$). The cloud absorption radiometer described in the following sections was designed to make angular intensity measurements from the zenith to nadir at selected wavelengths in the visible and near-infrared. Due to the monotonic nature of the intensity field in the diffusion domain, King (1981) proposed that the ratio of the zenith propagating to nadir propagating intensities be used to derive the spectral similarity parameter of clouds, thereby negating the need to have an absolute calibration of the instrument.

Analytic expressions relating the ratio of the zenith to nadir propagating intensity to each of the parameters A_g, s and $(1 - g)(\tau_c - \tau)$ have been derived by King and will not be repeated here. These formulae, which apply when $(1 - g)(\tau_c - \tau) \gtrsim 2.5$, permit an easy interpretation of spectral measurements of the zenith and nadir intensities within a cloud for arbitrary surface albedo without resorting to time-consuming radiative transfer computations. Furthermore, these expressions show that the intensity ratio is not a function of the

extraterrestrial solar flux density or solar zenith angle, although these parameters do affect the absolute magnitude of the intensity field.

By assuming that there is no absorption by the cloud particles at the visible wavelength for which the ratio of the zenith to nadir propagating intensities is the largest, and by assuming (or otherwise determining) A_g, one can use the intensity ratio at this wavelength to determine the scaled optical thickness between the flight level and the base of the cloud $[(1 - g)(\tau_c - \tau)]$. In addition, since the intensity must be a linear function of the cosine of the zenith angle in the diffusion domain at this wavelength, regardless of the value of the surface albedo, an angular scan from zenith to nadir can be used to verify that the observations are indeed within the diffusion domain. This ability to determine from the measurements themselves whether the diffusion domain has been reached is a very important feature of the diffusion domain method. With $(1 - g)(\tau_c - \tau)$ thus determined from an intensity ratio measurement in the visible wavelength region, the similarity parameter s can be determined as a function of wavelength from intensity ratio measurements at other wavelengths where water (or ice) absorbs solar radiation.

At some wavelengths, absorption by water vapor is expected to be the dominant absorbing constituent in clouds, while at other wavelengths absorption by liquid water is expected to be dominant. Twomey and Seton (1980) have shown that the wavelengths where water vapor absorbs solar radiation are generally shifted from the wavelengths where water droplets absorb radiation, thereby permitting one to select wavelengths in the design of a spectral radiometer that avoid the molecular absorption bands. As a consequence of this selection, one expects that any absorption inferred from measurements at these selected wavelengths is due solely to water or ice particles and aerosol particles.

Figure 2 illustrates the similarity parameter as a function of wavelength for a model cloud composed of water droplets only (solid curve) and droplets plus saturated vapor at −3.9°C (dashed curve). For the water droplet computations the cloud was assumed to have a particle size distribution proportional to $r^6 \exp(-1.6187r)$, where r is the particle radius in μm. This distribution of particles is a gamma distribution with an effective radius $r_{\text{eff}} = 5.56$ μm and an effective variance $v_{\text{eff}} = 0.111$ and is considered typical of fair weather cumulus clouds (Hansen, 1971). The water droplets were assumed to be spherical particles having the complex refractive indices tabulated by Hale and Querry (1973) for wavelengths in the range $0.25 \leq \lambda \leq 0.69$ μm, Palmer and Williams (1974) for $0.69 < \lambda \leq 2.0$ μm, and Downing and Williams (1975) for $\lambda > 2.0$ μm. For a different droplet size distribution, Twomey and Bohren (1980) have shown that the similarity parameter varies in direct proportion to $r_{\text{eff}}^{1/2}$.

For the water vapor calculations presented in Fig. 2 we have assumed a cloud of approximately 2 km thickness, with a cloud top located at 716 mb and a cloud base at 916 mb. This corresponds to the conditions of the aircraft observations of 30 May 1984, discussed in section 5. Using the observed cloud top and cloud base temperatures of −8.0°C and 0.5°C, respectively, and assuming the cloud to be composed of saturated vapor ($\bar{q}_s = 3.5$ g kg^{-1}), we obtain a value for the column loading of water vapor $w = 0.725$ g cm^{-2}. After applying the necessary pressure and temperature scaling to w, water vapor transmission functions were computed for this cloud layer at a resolution of 20 cm^{-1} using LOWTRAN 5 (Kneizys et al., 1980). The absorption optical depths thus obtained were combined with the corresponding optical properties for cloud droplets, where we further assumed that the cloud optical thickness $\tau_c = 64$ at a wavelength of 0.754 μm.

From these results it is evident that six different water vapor absorption bands occur in the visible and near-infrared regions, though the magnitude of these absorption bands varies as a function of w and τ_c. In order to concentrate on the absorption properties of water or ice particles and aerosol particles, thirteen channels were selected for the cloud absorption radiometer. These channels, shown on the top scale of Fig. 2, were chosen in order to define the absorption characteristics of all water vapor window regions in the near-infrared. Although the conversion from similarity parameter to single scattering albedo is not unique, due to the moderate spectral variation of g, we have included a single scattering albedo scale in the figure for those more accustomed to this parameter. The conversion from s to ω_0 illustrated in Fig. 2 applies to $\lambda = 0.754$ μm. The objectives of the experiment are therefore to experimentally determine s as a function of wavelength for the 13 channels of the cloud absorption radiometer and to compare these measurements to corresponding theoretical predictions for a cloud having the measured droplet size distribution. From such a comparison one can readily assess the magnitude and spectral variation of any anomalous absorption, if present. It is important to emphasize, however, that the experimental determination of s as a function of wavelength does not itself require a knowledge of the droplet size distribution.

3. Instrument description

The cloud absorption radiometer is a 13-channel scanning radiometer whose band center and bandwidth characteristics are summarized in Table 1. The instrument was designed to scan from 5° before zenith to 5° past nadir (190° aperture). Each scan of the instrument lies across the line that defines the aircraft track and extends up to 95° on either side of the aircraft horizon. This permits observations of both zenith and nadir directions with as much as a 5° aircraft roll. A detailed description of the optical, mechanical and electrical design of the radiometer follows.

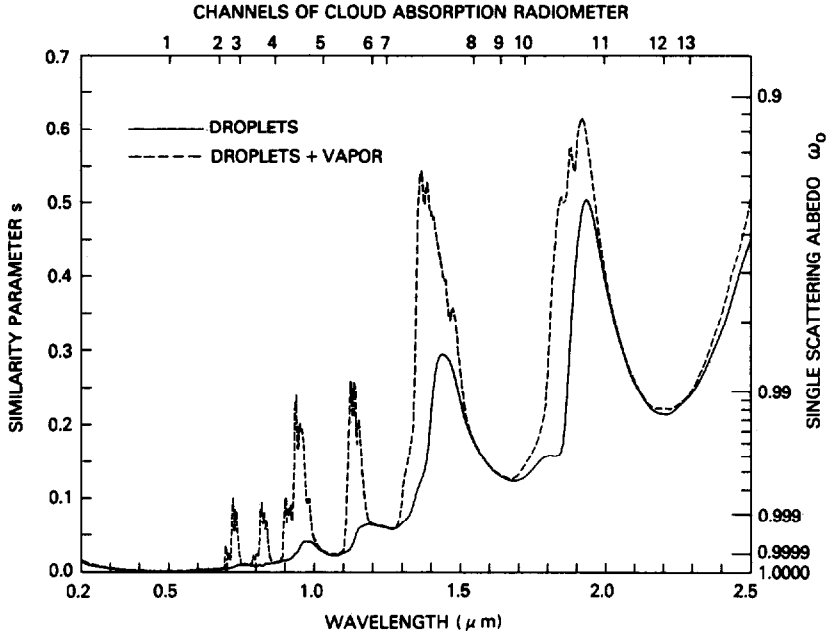

FIG. 2. Similarity parameter as a function of wavelength for water droplets alone (solid line) and drops plus vapor (dashed line). The 13 channels of the cloud absorption radiometer are identified on the upper scale. The single scattering albedo scale is valid at $\lambda = 0.754$ μm, where the cloud asymmetry factor is $g = 0.843$ for the cloud model assumed here.

a. Optics

The optical system of the cloud absorption radiometer is nondispersive, being composed of a complex configuration of dichroic beam splitters and narrowband interference filters similar to the cloud radiometer described by Curran et al. (1981). Figure 3 shows a cutaway drawing of the cloud absorption radiometer, which consists of a forward portion containing the optical system and electronics and a rear portion containing the scan mirror and telescope. The initial elements of the optical path are a 12.4 cm by 17.5 cm scan mirror, canted 45° to the long axis of the instrument, followed by a 12.4 cm Dall-Kirkham (Cassegrainian) telescope. These two elements define the scan geometry and field of view of the radiometer. The primary and secondary mirror system of the telescope houses a specially designed baffle system that virtually eliminates stray light from outside the instantaneous field of view of the instrument (cf. Fig. 3). The instantaneous field of view of the radiometer is 1° (17.5 mrad) while its total field of view is 190° along the scan line and 1° along the plane's velocity vector.

TABLE 1. Spectral characteristics, minimum intensities and corresponding minimum signal-to-noise ratios of cloud absorption radiometer channels.

Optical channel	Central wavelength (μm)	Spectral resolution (μm)	Minimum intensity* (mW cm^{-2} μm^{-1} sr^{-1})	Signal-to-noise ratio
1	0.503	0.016	1.085×10^{1}	3622
2	0.673	0.020	8.684×10^{0}	1903
3	0.744	0.019	7.268×10^{0}	2785
4	0.866	0.020	5.404×10^{0}	3022
5	1.031	0.020	3.884×10^{0}	3052
6	1.198	0.022	2.382×10^{0}	624
7	1.247	0.046	2.244×10^{0}	2446
8	1.547	0.030	4.502×10^{-1}	436
9	1.640	0.041	6.091×10^{-1}	685
10	1.722	0.038	4.470×10^{-1}	340
11	1.996	0.039	7.494×10^{-3}	29
12	2.200	0.040	7.708×10^{-2}	191
13	2.289	0.023	5.135×10^{-2}	33

* The minimum intensities $I(\tau_c, \tau; u, \mu_0)$ were computed assuming $\tau_c = 64$, $\tau = 32$, $u = \cos\theta = -1$, $\mu_0 = 0.5$ and $A_g = 0$.

As shown in Figs. 3 and 4, the radiation, having left the secondary telescope mirror, first passes through the defining field-stop and then through a pair of specially designed dichroic beam splitters. The spectrally broad wavelength interval transmitted through these dichroics enters branch III, where it is further defined spectrally by a filter wheel containing six narrowband interference filters. The radiation reflected by the first dichroic (D1) enters branch I. This radiation is defined spectrally by a series of beam splitters, mirrors and narrowband interference filters, and consists of radiation in the wavelength range $0.50 \leqslant \lambda \leqslant 0.87$ μm. The radiation transmitted by D1 and reflected by the second dichroic D2 enters branch II, where it is separated into three channels in a similar manner. This section contains filters in the 1.03 to 1.25 μm interval. The radiation trans-

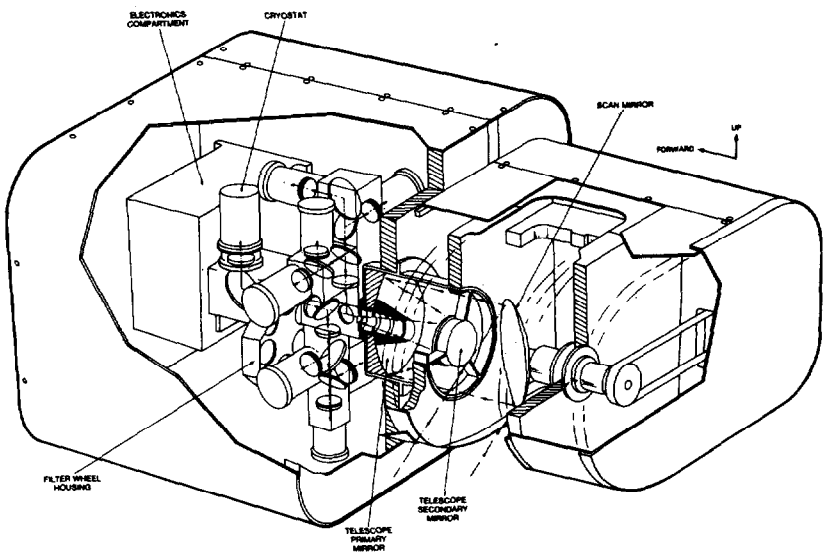

FIG. 3. Cutaway drawing of the cloud absorption radiometer. The instrument housing is approximately 72 cm long, 41 cm wide and 39 cm deep.

mitted through D2 forms branch III, which incorporates a filter wheel that is periodically rotated to measure a new wavelength interval. With this configuration the first seven channels are continuously and simultaneously sampled, while the eighth registered (electrical) channel is selected from among the six channels on the filter wheel. Channels 1–5 use hybrid silicon photodiodes operating at 308 K, channels 6–7 use germanium detectors operating at 255 K, and the remaining channels, selected by the filter wheel, use an indium antimonide (InSb) cold-filtered detector cryogenically cooled to 77 K.

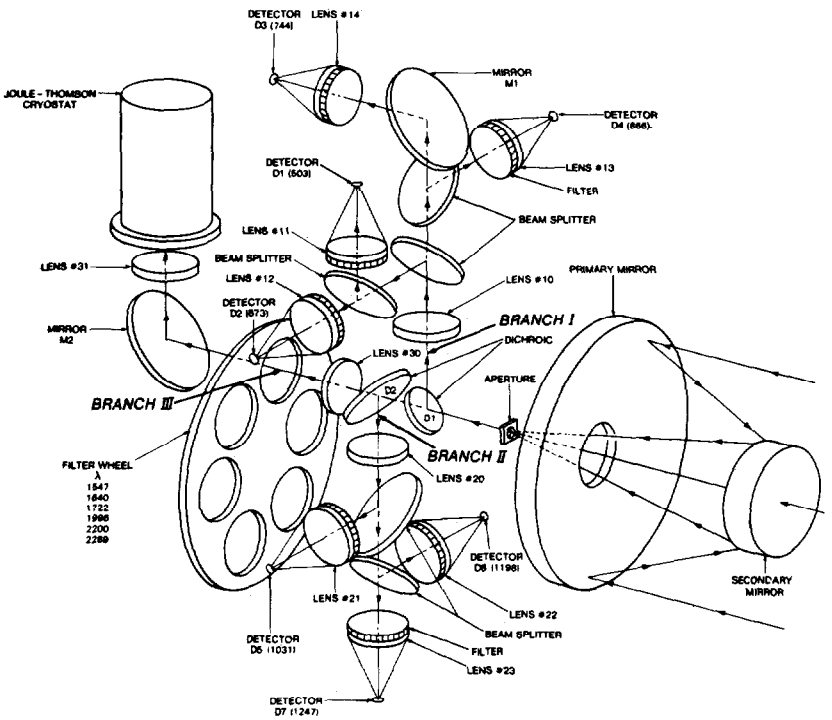

FIG. 4. Schematic illustration of the cloud absorption radiometer optical system.

b. Mechanical design

The forward portion of the cloud absorption radiometer, which contains the optical system and electronics, is housed in a compact 39 cm × 41 cm × 37 cm tunneled aluminum block. Prior to May 1984 the cloud absorption radiometer was mounted in the tail portion of the University of Washington's B-23 cloud and aerosol research aircraft (see Fig. 5). The rear portion of the radiometer containing the scan mirror and telescope extended 34 cm past the tail of the aircraft, with a cross section of 27 cm × 35 cm. As shown in Fig. 5, the cloud absorption radiometer contains a door mechanism for closing the entrance aperture during takeoff and landing, and a shroud around the forward portion of the radiometer for reducing turbulence around the entrance aperture.

In order to reduce the potential for condensation on the optical components of the radiometer, the instrument contains heating elements attached to the back of the telescope primary and secondary mirrors and scan mirror to raise the temperature of the mirrors above ambient levels. In addition, warm dry cabin air is forced through the forward section of the radiometer to further reduce the possibility of condensation on the optics during flight. To assure that the scan mirror is free of condensed water, a small incandescent lamp illuminates the mirror once per mirror revolution with a detector designed to distinguish between the strong specular reflection of a clean mirror and a reduced diffuse reflection in the event of condensation on the mirror. In practice this proved to be of value in indicating intervals of bad or questionable data, especially when the cloud liquid water content exceeded 0.3 g m^{-3}.

Due to the small magnitude of the radiant intensity at many near-infrared wavelengths in the interior of optically thick clouds, it is necessary to apply a large amount of direct-coupled amplification to the detector outputs. A unique scheme was therefore developed to restore the output of each channel of the radiometer to a zero intensity reference during each 600 ms scan cycle, using a metal shutter to block the entrance aperture of the optical system. This innovation, made possible at least in part by the relatively low rotation rate of the scan mirror, eliminates baseline drift and reduces low-frequency noise. The use of a shutter to dc-restore the output signal contrasts with the more common practice of viewing an internal blackbody once per mirror revolution. The latter technique often suffers from errors arising from stray light illumination of the target.

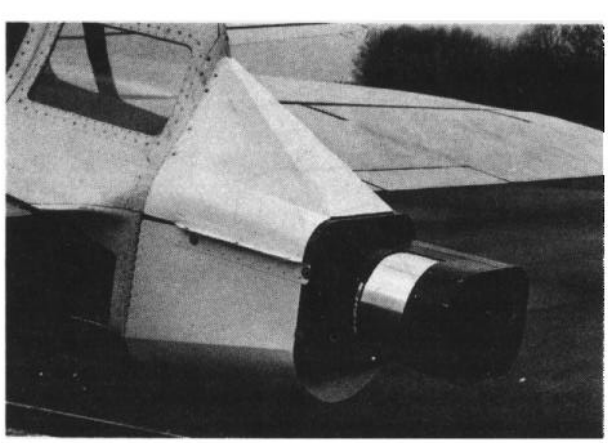

FIG. 5. Location of the cloud absorption radiometer in the tail of the University of Washington's B-23 aircraft.

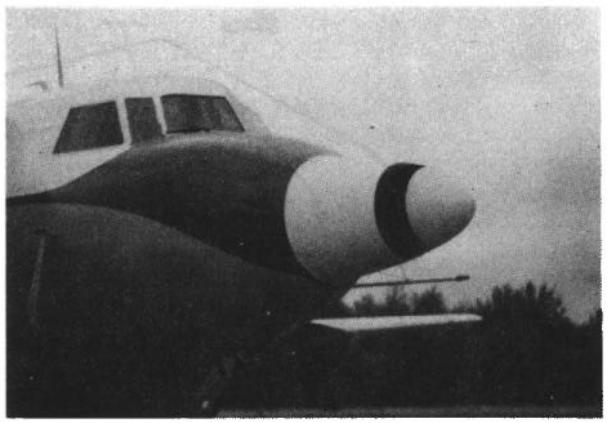

FIG. 6. Location of the cloud absorption radiometer in the nose of the University of Washington's C-131A aircraft.

After May 1985 the cloud absorption radiometer was mounted in the nose of the University of Washington's C-131A aircraft, with the portion of the radiometer containing the telescope and scan mirror extending out in front of the aircraft (see Fig. 6). A foam housing was constructed to surround the cloud absorption radiometer, with a single 190° opening cut to permit radiation to reach the entrance aperture. In the design of the new housing, particular attention was given to aerodynamic flow characteristics so that there was little opportunity for cloud water to impinge on the scan mirror and optical system. This has been confirmed by aircraft flights where condensation on the radiometer optics has not been observed, even in quite water-ladened clouds.

c. Electronics

The electronics functions of the cloud absorption radiometer are divided into two physical sections. These sections, identified in Fig. 7, are the scanner section and control module. Both aircraft supply 115 V ac, 60 Hz power and 28 V dc power. The dc power is used for controlling detector temperatures and for heating the anticondensation optics. The only portion of the scanner section of Fig. 7 which is not physically located inside the cloud absorption radiometer is the high pressure N_2 gas bottle and regulator. This supplies 2000 psi (13790 kPa) gas to the Joule-Thomson cryostat that cools the 77 K InSb detector of channels 8–13.

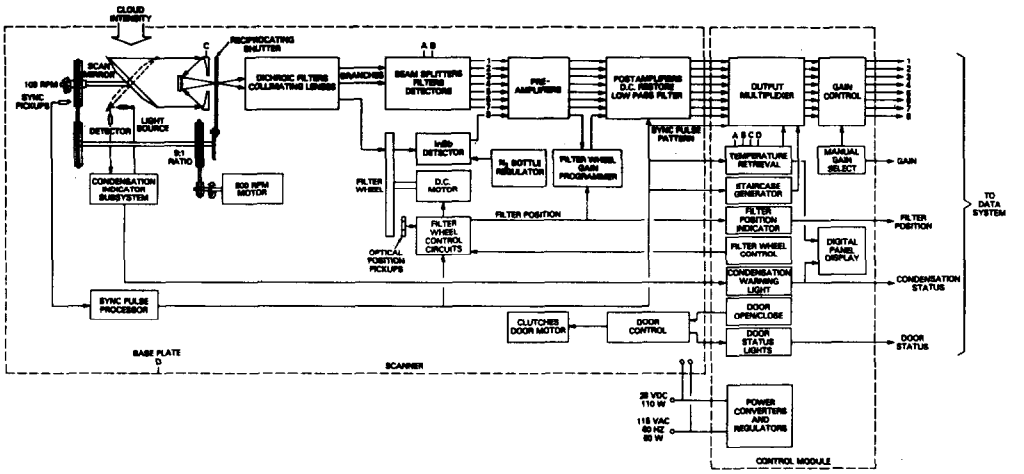

FIG. 7. Block diagram of the electronics associated with the cloud absorption radiometer. The electronics functions are housed in the scanner section and control module.

Due to the large variation in the absolute magnitude of the internal intensity field in the six filter wheel channels, it is necessary to amplify the signal output from the InSb detector by various gains, depending on which filter is in the optical path. This is accomplished using a filter wheel gain programmer circuit that automatically selects the required gain for each of the six filter wheel channels. In this manner, the output voltage of all eight electrical channels is kept at roughly the same level. To allow for the large variations in absolute magnitude of the intensity arising as a function of cloud optical thickness and, especially, solar zenith angle, the control panel provides for manual gain selection that applies a uniform gain adjustment to all eight electrical channels simultaneously. This manual gain setting, which permits greater flexibility in field operations, is output to the data system. Adequate gain stability is ensured by temperature regulation of the preamplifiers and by the use of stable film-type resistors in all gain stages.

Following amplification, the detector signals are filtered by a two-pole low-pass filter. The resulting analog signals are then multiplexed to incorporate start and end scan sync pulses, thermistor temperatures and a calibration voltage staircase for converting digital counts to voltage. There are four thermistors labeled A–D in the scanner module of Fig. 7. These thermistors measure the temperatures of the primary mirror of the telescope (A), optics (B–C), and baseplate (D).

4. Calibration

Radiometric calibration is obtained by observing a laboratory standard source consisting of a 6-ft diameter (182.5 cm) integrating sphere maintained at the Goddard Space Flight Center. The sphere is coated with a highly reflective $BaSO_4$ paint and internally illuminated by a series of up to 12 quartz-halogen lamps. The cloud absorption radiometer is placed at the entrance of a 25-cm opening on the side of the sphere, where it views the highly lambertian radiation exiting the sphere. The magnitude of the intensity incident on the radiometer can be varied by changing the number of lamps illuminating the interior of the sphere, or by introducing neutral density filters in the path of the outgoing radiation. The spectral intensity at the opening of the sphere is periodically compared to secondary calibration sources maintained at the National Bureau of Standards. The spectral intensity of the sphere is thought to have an absolute accuracy of about ±4%, an accuracy that is sufficient for the cloud absorption experiment since it depends on relative, rather than absolute, intensity measurements. The cloud absorption radiometer is calibrated by measuring its output voltage in each channel as a function of spectral intensity for varying illumination levels from the sphere. These measurements permit the gain to be adjusted for each channel and allow the linearity of the instrument to be verified over the dynamic range of the expected signal levels.

Prior to conducting the first flight campaign, radiative transfer calculations were performed for a wide variety of conditions in the diffusion domain of optically thick clouds. These computations were performed using formulae presented by King (1981), together with asymptotic functions and constants derived from the asymptotic fitting method of van de Hulst (1968). The cloud similarity parameters used in these computations were the same ones illustrated in Fig. 2. Table 1 presents computations of the intensities at the midlevel of a cloud layer of total optical thickness $\tau_c = 64$ when the solar zenith angle $\theta_0 = 60°$ ($\mu_0 = 0.5$). These intensities were computed for radiation propagating in the vertical direction when $A_g = 0$, thereby representing the *minimum* intensity for an angular scan. The gains of individual channels of the cloud absorption radiometer were adjusted using these results as well as comparable

results obtained for other cloud optical properties, surface albedos, observation angles and solar zenith angles. Based on these computations, as well as measurements from the integrating sphere, we were able to assure that meaningful signal levels could be obtained in the vast majority of optically thick clouds.

In bench tests of the radiometer output, the peak-to-peak noise level was ≤ 5 mV for channels 1–5 and 7; 17–20 mV for channels 6, 8, and 9; 30–35 mV for channels 10–12; and 200 mV for channel 13, all out of a maximum signal of 10 V. These noise measurements, together with the calibration coefficients of the radiometer and the intensity computations presented in Table 1, result in the root-mean-square values of the signal-to-noise ratios presented in the final column of Table 1. Larger signal-to-noise ratios are expected for observations in optically thinner clouds, at smaller solar zenith angles, over nonzero surface albedos and at other observation zenith angles.

To maintain a check on the calibration in the field, a light box target is used prior to each flight. This target is a calibrated, near-lambertian, portable light source consisting of four 45 W quartz-iodide lamps mounted under an opal diffuser and surrounded by walls coated with $BaSO_4$. A special feedback control system utilizes a temperature-controlled reference photodiode to maintain light intensity constant over time, despite large changes in power line voltage and ambient temperature. Most importantly, this control provides rapid stabilization so that the intensity may be rapidly stepped to several known levels. In practice, the test source steps automatically through 10 preset levels and the corresponding outputs for all 13 channels of the cloud absorption radiometer are recorded on the start of each flight data tape.

5. In-flight performance

The cloud absorption radiometer, developed by Goddard Space Flight Center, and the data acquisition system, developed by the University of Washington, were flown on the Douglas B-23 aircraft from January–May 1984, and on the Convair-131A aircraft from May 1985–present. The radiometer was flown as one of a group of instruments that included upward- and downward-looking pyranometers, cloud microphysics probes (Knollenberg 1-D and 2-D cloud and precipitation probes and a Johnson–Williams hot-wire device for measuring the cloud liquid water content) and an air batch sampler for measuring the cloud interstitial aerosol size distribution. Detailed descriptions of these instruments can be found in Coulson (1975), Knollenberg (1981) and Radke (1983), respectively.

An example of multiplexed digital data for three scan lines of the cloud absorption radiometer is shown in Fig. 8. These data were acquired in a mixed-phase stratocumulus cloud over Puget Sound, Washington on 30 May 1984. The stratocumulus layer was about 2 km thick with a cloud base at ~900 m MSL. Included in each scan of Fig. 8 are two sync pulses denoting the start and end of the active scan segment. These pulses are distinguished by their differing widths. Also multiplexed into each channel on each scan cycle are a set of reference voltages as well as measurements from the four thermistors discussed in section 3c. The reference voltages range from 0.00 to 8.00 V in steps of 1.00 V and give the appearance of a staircase. This voltage staircase permits the conversion from digital counts to voltage, while the conversion from voltage to intensity is accomplished through the calibration procedure described in the preceding section. The scan rate of the cloud absorption radiometer scan mirror is 1.67 Hz, resulting in a scan duration of 600 ms (cf. Fig. 8).

The active scan data presented in Fig. 8 correspond to outputs from electrical channels 1, 6 and 8. The optical channel in the filter wheel position was channel 8 ($\lambda = 1.547$ μm) for the first scan and channel 9 ($\lambda = 1.640$ μm) for the third scan, with the middle scan corresponding to the lost scan during which the filter wheel was rotating. As one can see on careful examination of Fig. 8, the time required for the filter wheel to rotate from one position to the next is about 350 ms, and thus the last portion of data in the middle scan is valid data for the new filter wheel position (in this case channel 9). The cloud absorption radiometer is normally operated with four scans of data being collected in each position of the filter wheel before it rotates to the next position. The control panel allows this dwell interval to be altered from one to eight scans per filter, or the filter wheel to be manually indexed to a particular channel. With automatic sequencing, each minute of flight duration results in 100 measurements of the zenith and nadir intensities for each of the first seven channels and typically 12 measurements for each of the six filter wheel channels. Due to sufficiently large signal-to-noise ratios in the measurements, no smoothing of the data presented in Fig. 8 was required.

Examination of the active scan data of Fig. 8 shows that the angular distribution of intensity in channel 1 varies as $I(\tau, \cos\theta) = a + b\cos\theta$, as required theoretically for measurements made in the diffusion domain of a conservative scattering cloud ($\omega_0 = 1$, $s = 0$). Furthermore, the angular distribution of intensity departs increasingly from a cosine function as the absorption increases. This is especially evident in the active scan data for channels 8 and 9, where the more isotropic variation of intensity toward the nadir (vertically propagating) direction is quite consistent with the expectations of Fig. 1. Although the microphysics data showed this cloud to be partially composed of ice, this is not at all evident in the diffusion domain measurements due to the high degree of multiple scattering.

6. Conclusions

We have described the design of a radiometer for making airborne measurements of the angular distribution of scattered radiation deep within a cloud layer.

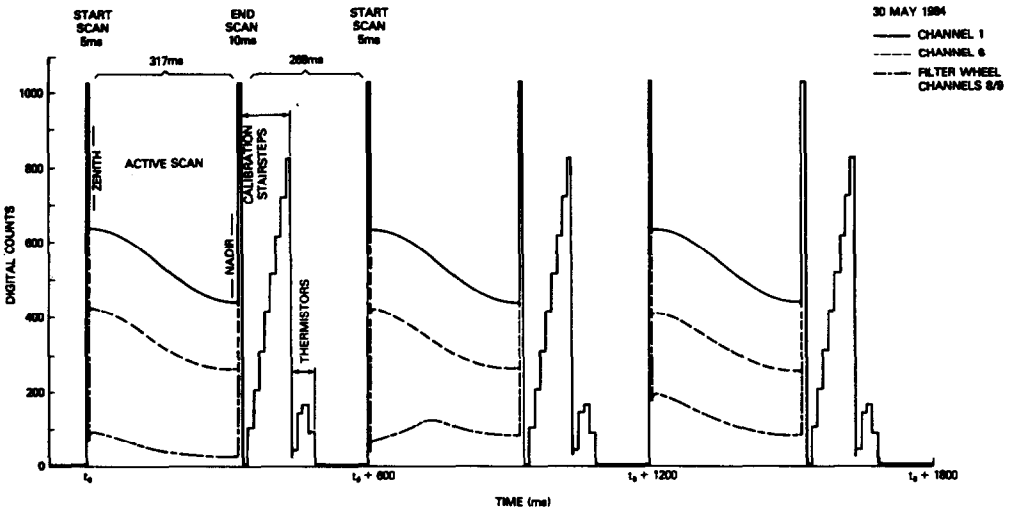

FIG. 8. An example of digital output of the cloud absorption radiometer as a function of time for three scans taken in a stratocumulus cloud layer in Puget Sound, Washington, on 30 May 1984. Each scan consists of a start scan pulse, an active scan region where the intensity varies smoothly from zenith to nadir, an end scan pulse, a calibration staircase and 4 thermistor measurements. Data for three electrical channels are illustrated, where the data in the middle scan include the rotation of the filter wheel.

This instrument was developed for the purpose of determining the similarity parameter of clouds as a function of wavelength using the diffusion domain method introduced by King (1981). This method makes use of the ratio of the zenith-propagating to nadir-propagating intensities in the diffusion domain of an optically thick, horizontally extensive cloud, and as such is not critically dependent on the absolute calibration of the instrument. The optical, mechanical and electrical design characteristics of the cloud absorption radiometer have been described, together with a description of preflight and laboratory calibration checks. Finally, selected results from a supercooled stratocumulus cloud over Puget Sound, Washington, have been presented to highlight the instrument performance.

The cloud absorption radiometer is the first airborne scanning radiometer to be developed for measuring the spectral and angular distribution of scattered radiation inside clouds. This radiometer complements reflected solar radiation measurements obtained using spectral radiometers flown above clouds, such as those described by Curran et al. (1981), Twomey and Cocks (1982) and Stephens and Scott (1985).

McCormick (1985) has recently proposed that angular intensity measurements be made at two different altitudes in the diffusion domain for the purpose of deriving the spectral similarity parameter of clouds. Unlike the diffusion domain method of King (1981), McCormick's method does not require an assumption about cloud absorption properties at any wavelength, since a combination of intensity measurements from different altitudes eliminates the need to know the cloud optical thickness. On the other hand, it suffers from the disadvantage of requiring measurements in temporally varying clouds at two different altitudes and requires that the clouds be optically thicker. Duracz and McCormick (1986) have shown, in addition, that the diffusion domain method of King (1981) is more sensitive to the similarity parameter for weakly absorbing clouds (or wavelengths), while the two-altitude approach of McCormick (1985) has its greatest appeal at wavelengths where the cloud is more strongly absorbing. The cloud absorption radiometer will be used to collect data to test both of these approaches, where possible, and the results of these applications will be reported in future contributions.

Although the diffusion domain method, in its simplest form, requires the assumption that the cloud is nonabsorbing at some wavelength in the visible region, this assumption is necessary solely for the purpose of estimating the scaled optical thickness between the aircraft flight level and the base of the cloud $[(1 - g)(\tau_c - \tau)]$. Since this parameter becomes less important as the optical thickness increases and as the similarity parameter (absorption) increases, this assumption is not expected to have a strong influence on the derived similarity parameter at wavelengths in the near-infrared. Furthermore, estimates of $(1 - g)(\tau_c - \tau)$ can be obtained from ancillary information, thereby reducing the importance of the assumption that $s = 0$. The use of analytic formulae in the analysis of the internal intensity ratio measurements permits a straightforward error propagation analysis to be performed on the results, thereby permitting the effects of this assumption to be readily examined. These results will be presented in a later contribution in which we present an analysis of data obtained with the cloud absorption radiometer.

Acknowledgments. The authors are grateful for the many contributions of the Cloud and Aerosol Research

Group, Department of Atmospheric Sciences, University of Washington. We are especially grateful to P. V. Hobbs and L. F. Radke for scientific collaboration and data collection, J. D. Russell for developing the data acquisition system, and D. O. Veach for integrating the cloud absorption radiometer on the B-23 and C-131A aircraft.

This research was supported, in part, by funding from the National Science Foundation (Grant ATM-82-18978).

REFERENCES

Coulson, K. L., 1975: *Solar and Terrestrial Radiation,* Academic Press, 322 pp.

Curran, R. J., H. L. Kyle, L. R. Blaine, J. Smith and T. D. Clem, 1981: Multichannel scanning radiometer for remote sensing cloud physical parameters. *Rev. Sci. Instrum.*, **52,** 1546–1555.

Davies, R., W. L. Ridgway and K. E. Kim, 1984: Spectral absorption of solar radiation in cloudy atmospheres: A 20 cm^{-1} model. *J. Atmos. Sci.*, **41,** 2126–2137.

Downing, H. D., and D. Williams, 1975: Optical constants of water in the infrared. *J. Geophys. Res.*, **80,** 1656–1661.

Duracz, T., and N. J. McCormick, 1986: Equations for estimating the similarity parameter from radiation measurements within weakly absorbing optically thick clouds. *J. Atmos. Sci.*, **43,** 486–492.

Hale, G. M., and M. R. Querry, 1973: Optical constants of water in the 200-nm to 200-μm wavelength region. *Appl. Opt.* **12,** 555–563.

Hansen, J. E., 1971: Multiple scattering of polarized light in planetary atmospheres. Part I. The doubling method. *J. Atmos. Sci.*, **36,** 508–518.

Henyey, L. C., and L. J. Greenstein, 1941: Diffuse radiation in the galaxy. *Astrophys. J.*, **93,** 70–83.

Herman, G. F., 1977: Solar radiation in summertime arctic stratus clouds. *J. Atmos. Sci.*, **34,** 1423–1432.

——, and J. A. Curry, 1984: Observational and theoretical studies of solar radiation in arctic stratus clouds. *J. Climate Appl. Meteor.*, **23,** 5–24.

King, M. D., 1981: A method for determining the single scattering albedo of clouds through observation of the internal scattered radiation field. *J. Atmos. Sci.*, **38,** 2031–2044.

Kneizys, K. X., E. P. Shettle, W. O. Gallery, J. H. Chetwynd, Jr., L. W. Abreu, J. E. A. Selby, R. W. Fenn and R. A. McClatchey, 1980: Atmospheric transmittance/radiance: Computer code LOWTRAN 5. AFGL-TR-80-0067, Air Force Geophysics Laboratories, Hanscom AFB, 233 pp.

Knollenberg, R. G., 1981: Techniques for probing cloud microstructure. *Clouds: Their Formation, Optical Properties, and Effects,* P. V. Hobbs and A. Deepak, Eds., Academic Press, 15–89.

McCormick, N. J., 1985: Methods for estimating the similarity parameter of clouds from internal measurements of the scattered radiation field. *J. Quant. Spectrosc. Radiat. Transfer,* **33,** 63–70.

Mel'nikova, I. N., 1978: The field of scattered solar radiation in a cloud layer. *Izv. Acad. Sci., USSR, Atmos. Ocean. Phys.*, **14,** 928–931.

Newiger, M., and K. Bähnke, 1981: Influence of cloud composition and cloud geometry on the absorption of solar radiation. *Contrib. Atmos. Phys.*, **54,** 370–382.

Palmer, K. F., and D. Williams, 1974: Optical properties of water in the near infrared. *J. Opt. Soc. Amer.*, **64,** 1107–1110.

Radke, L. F., 1983: Preliminary measurements of the size distribution of cloud interstitial aerosol. *Precipitation Scavenging, Dry Deposition and Resuspension,* H. R. Pruppacher, R. G. Semonin and W. G. N. Slinn, Eds., Elsevier, 71–78.

Reynolds, D. W., T. H. Vonder Haar and S. K. Cox, 1975: The effect of solar radiation absorption in the tropical troposphere. *J. Appl. Meteor.*, **14,** 433–444.

Rozenberg G., M. Malkevich, V. Malkova and V. Syachinov, 1974: Determination of the optical characteristics of clouds from measurements of reflected solar radiation by KOSMOS 320. *Izv. Acad. Sci. USSR, Atmos. Ocean. Phys.*, **10,** 14–24.

Slingo, A., and H. M. Schrecker, 1982: On the shortwave radiative properties of stratiform water clouds. *Quart. J. Roy. Meteor. Soc.*, **108,** 407–426.

Stephens, G. L., 1978a: Radiation profiles in extended water clouds. I: Theory. *J. Atmos. Sci.*, **35,** 2111–2122.

——, 1978b: Radiation profiles in extended water clouds. II. Parameterization schemes. *J. Atmos. Sci.*, **35,** 2123–2132.

——, and J. C. Scott, 1985: A high speed spectrally scanning radiometer (SPERAD) for airborne measurements of cloud optical properties. *J. Atmos. Oceanic Tech.*, **2,** 148–156.

——, G. W. Paltridge and C. M. R. Platt, 1978: Radiation profiles in extended water clouds. III: Observations. *J. Atmos. Sci.*, **35,** 2133–2141.

Twomey, S., 1972: The effect of cloud scattering on the absorption of solar radiation by atmospheric dust. *J. Atmos. Sci.*, **29,** 1156–1159.

——, 1976: Computations of the absorption of solar radiation by clouds. *J. Atmos. Sci.*, **33,** 1087–1091.

——, 1977: The influence of pollution on the shortwave albedo of clouds. *J. Atmos. Sci.*, **34,** 1149–1152.

——, 1983: Radiative effects in California stratus. *Contrib. Atmos. Phys.*, **56,** 429–439.

——, and C. F. Bohren, 1980: Simple approximations for calculations of absorption in clouds. *J. Atmos. Sci.*, **37,** 2086–2094.

——, and K. J. Seton, 1980: Inferences of gross microphysical properties of clouds from spectral reflectance measurements. *J. Atmos. Sci.*, **37,** 1065–1069.

——, and T. Cocks, 1982: Spectral reflectance of clouds in the near-infrared: Comparison of measurements and calculations. *J. Meteor. Soc. Japan,* **60,** 583–592.

Van de Hulst, H. C., 1968: Asymptotic fitting, a method for solving anisotropic transfer problems in thick layers. *J. Comput. Phys.*, **3,** 291–306.

Wiscombe, W. J., R. M. Welch and W. D. Hall, 1984: The effects of very large drops on cloud absorption. Part I: Parcel models. *J. Atmos. Sci.*, **41,** 1336–1355.